# Improved Energy Storage Solution Based on Hybrid Oxide Materials

María C. López, Gregorio F. Ortiz,* Pedro Lavela, Ricardo Alcántara, and José L. Tirado

Inorganic Chemistry Laboratory, University of Cordoba, Campus of Rabanales, Marie Curie Building, 14071 Cordoba, Spain

ABSTRACT: Electrodeposited-oxidized FeCoNi-based electrodes have shown to exhibit enhanced electrochemical behavior in Li cells in terms of first-cycle reversibility and minimal discharge polarization on successive discharges. The latter is referred to as the main faradic conversion reaction taking place at 0.8 V versus Li^+/Li^0 in first and consecutive cycling. In this communication, the faradic and capacitive charge-storage capacities are unfolded. The main effect responsible for the high reversibility achievable from first to second discharge is a pseudocapacitive contribution that starts in the second discharge between 1.75 and 1.5 V and compensates for the loss of capacity due to electrolyte decomposition in the previous discharge, thus leading to a high Coulombic efficiency (~85%). The intensity dependence of the different peak currents with the sweep rate has been extensively examined to understand the differences of capacity contributions in the total charge storage. Specific capacitance for FeCoNi-based film could reach as high as 600 F g^{-1}.

KEYWORDS: Li-battery, FeCoNi alloys, Oxidized electrodes, Capacitive storage, Faradic capacity
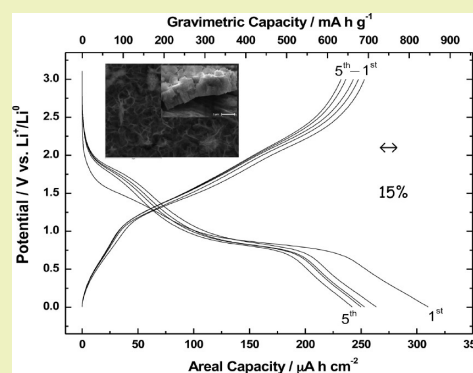
INTRODUCTION

Transition metal oxides (Fe, Co, Ni, etc.) are of significant interest as promising alternatives for inexpensive electrode materials in both types of energy-storage systems: supercapacitors and Li-ion batteries. On the one hand, the notable pseudocapacitive behavior of particular oxide materials leads to superior electrochemical capacitive properties.[1−4] For instance, by simply controlling particle shape and porosity, a capacitance of 110 F g^{-1} is achievable for Co_3O_4 with 80−120 m^2 g^{-1} specific surface area.[4] On the other hand, faradic reactions that cobalt oxide undergoes in Li-batteries were as well described in the beginning of the 21st century as a "conversion reaction" where transition metal oxide is reduced with lithium (discharge) and reoxidized (charge), providing subsequently as much as 700 mA h g^{-1}, twice the gravimetric capacity of graphite.[5] The reduction process is given by a voltage plateau whose extension or length (associated to the faradic capacity) is usually equivalent to the number of electrons required to fully reduce the compound, thus forming nanometric metal (M) particles surrounded by a Li_2O matix. Additional capacity in the tail of the curve at low potential is usually observed just after the conversion reaction, and this contribution is tentatively attributed to a capacitive-like behavior[6] or to the formation of the gel-like polymeric film from the electrolyte decomposition.[7] The former is confirmed by theoretical calculations and based on a two-phase capacitive behavior at the M/Li_2O interfaces in the reduced electrodes, which would allow for the storage of Li^+ ions on the Li_2O side and electrons on the M side.[6,8,9] Upon charge, formation of the initial transition metal oxide is expected, but drastic changes (decrease) in the particle size and structure of initial oxide have been suggested in earlier work.[6−9] This fact is reflected in a large hysteresis and in how the amount of energy released in the oxidation differs significantly from that needed for reduction. One of the possible origins of such different energy used to reduce-oxidize the metal comes from the large amount of interfacial surface generated in first discharge. So, the design of nanoparticles and nanomaterials and the study of their interfaces may be the next step to open new perspectives for understanding this type of reaction.

The application of nanostructured materials with tailored morphologies, chemistry, and physical properties to electrochemical devices (batteries or supercapacitors) is being intensively studied in order to provide enhanced energy density systems without compromising their inherent high power density and cyclability. Those electrode materials that exploit physical adsorption or redox reactions of electrolyte ions are foreseen to bridge the performance disparity between batteries with high energy density and capacitors with high power density. Indeed, nanomaterials have been recognized for their great application as high performance electrode materials of electrochemical supercapacitors[10−12] and batteries[13−15] because they can improve the power capabilities and life cycles owing to the high surface area and fast electrical pathways related to their unique structure and shape. However, there are several aspects as the voltage polarization and Coulombic inefficiency that needs to be understood and resolved (if possible) from a fundamental point of view. In this regard, our group announced pioneering studies related to the enhanced electrochemical properties on the mechanism of reaction found in ternary FeCoNi oxidized alloys.[15] In the present work, we describe the fabrication of oxide materials having hybrid charge-storage properties by simple and versatile electrochemical methods.

The materials are composed of first-row transition metals oxides, which are relatively abundant and inexpensive, to allow a sustainable application in energy storage.

Here, 2D oxidized FeCoNi-based porous films were grown on Ti substrates via a facile, low-cost, and effective electrochemical method corroborating the electrochemical behavior found in Li cells in an early report.[15] These metals do not alloy with Li, and their oxides have limited intercalation of Li ions; hence, the conversion reaction mechanism prevails. Furthermore, the origin of the stored capacity is investigated now by following similar approaches to other systems previously reported.[16,17] The voltammetric sweep rate dependence of current density is used to determine quantitatively the capacitive contribution. Then, we will show in which proportion the materials show different levels of capacitive charge storage and conversion capacities, having in mind that at nanoscale level the charge storage of cations from faradic processes occurring at the surface (cations electrochemically adsorb onto the surface through charge-transfer processes), referred to as pseudocapacitive effect,[18] is becoming increasingly important in these systems.

■ EXPERIMENTAL SECTION

The $Ni(NO_3)_2 \cdot 6H_2O$, $CoSO_4 \cdot 7H_2O$, and $FeSO_4 \cdot 7H_2O$ materials were purchased from Strem Chemicals (99.9%), Aldrich ($\geq$99%), and Panreac, respectively. The electrochemical deposition of FeCoNi film was carried out by galvanostatic experiments at room temperature (rt). A 0.02 M solution of each salt was used. A constant current density of -2.5 mA cm^{-2} during 240 s and alternatively 600 s was employed. A programmable galvanostat/potentiostat PGSTAT12 Autolab and Arbin instruments with a glass reference electrode (Ag/AgCl) and a platinum wire as counterelectrode were used. The deposits were obtained on 127 μm thick Ti foil (99.7% purity). The as-prepared deposits were treated at 450 °C in air for 2 h using a heating rate of 3.5 °C min^{-1}. Considering Faraday's law, the estimated mass for oxide electrodeposited is 0.18 mg per square centimeter if using a current of -2.5 mA cm^{-2} during a time of 240 s. From a practical point of view, Ti is more suitable than Al and Cu for electrodeposition of materials such as iron, nickel, or tin, as reported in previous works.[14,15] In this way, Al foils cannot be used because they form alloys with lithium in the voltage window in which the negative electrode works. Titanium does not form alloys with lithium and shows better corrosion resistance than Cu foils and good mechanical resistance. For comparative purposes, binary alloys such as FeCo, CoNi, and FeNi were prepared by following the same procedure as above. The mixture of commercial oxides was ground manually in an agate mortar.

Microstructure and surface morphology of the materials were characterized by using grazing-incidence small-angle X-ray diffraction (GISAXRD) patterns that were obtained in an EQ 31 04 Panalytical X'Pert PRO MPD system equipped with Mo Kα radiation, and scanning electron microscopy with a JEOL-SM6300 instrument. Transmission electron microscopy was used to fully characterize the structure of the film with a JEOL JEM 2100 instrument.

The chemical state and composition of the electrode materials were analyzed using ^{57}Fe Mössbauer spectra (MS) recorded with an EG & G constant accelerator spectrometer in transmission mode. The source was ^{57}Co in Rh matrix (10 mCi). The velocity scale was calibrated from the magnetic sextet of a high-purity iron foil absorber. Experimental data were fitted to Lorentzian lines by using a least-squares based method. The quality of the fit was controlled by the classical test of χ^2. All the isomer shifts are given relative to the center of the α-Fe spectrum at room temperature. Moreover, X-ray photoelectron spectroscopy (XPS) measurements were performed in a ultrahigh vacuum (UHV) multipurpose surface analysis system operating at pressures $< 10^{-10}$ mbar using a conventional X-ray source (XR-50, Specs, Mg, 1253.6 eV) in a "stop-and-go" mode to reduce potential damage due to sample irradiation. The survey and detailed

region high-resolution spectra (pass energy 25 and 12 eV, step size 1 and 0.1 eV, respectively) were recorded at room temperature with a Phoibos 150-MCD energy analyzer. Thin-film samples were placed on a sample holder using double-sided adhesive tape and subsequently evacuated under vacuum overnight. Eventually, the sample holder containing the degassed sample was transferred to the analysis chamber for XPS studies. Binding energies were referenced to the C 1s line at 284.9 eV from adventitious carbon. The curve deconvolution of the obtained XPS spectra was obtained using the "Casa" XPS program. Nitrogen adsorption−desorption isotherms were conducted on a Quantachrome-Nova instrument at 77 K. The sample was previously outgassed under vacuum at 250 °C.

The electrochemical characterizations were performed using Arbin and Bio-Logic MPG-2 multichannel potentiostat/galvanostat systems using a scan rate of 50 μA cm^{-2}. Schematically, the cell configuration can be summarized as Li/1 M LiPF$_6$ (EC/DEC = 1:1 in mass ratio)/ FeCoNi-based electrodes. The Li half cell consisted of two-electrode Swagelok type cells using a lithium disk as a counterelectrode. The working electrode disk had a diameter of 9 mm. The two electrodes were separated by glass fiber sheets (GF/A-Whatman) soaked in 1 M LiPF$_6$ (EC/DEC) acting as electrolyte. The Li test cells are assembled in a glovebox under a controlled argon atmosphere with moisture content, and the oxygen level was less than 2 ppm. For capacitive measurements cyclic voltammetry (CV) was performed in conventional three-electrode cells using a graphite rod as counterelectrode, a Hg/Hg$_2$SO$_4$ (SO$_4^=$ sat'd) as reference electrode, the electroplated FeCoNi-based samples as the working electrodes, and a solution of 1.5 M KOH as the electrolyte. Cyclic voltammograms were performed at room temperature between -0.65 and -0.05 versus Hg/Hg$_2$SO$_4$ (SO$_4^=$, sat'd) at various sweep rates ranging from 1 to 50 mV s^{-1}.

The electrochemical impedance analysis (EIS) was performed using an Autolab PGSTAT12 system. For this purpose, a three-electrode configuration is used in which FeCoNi-based electrode acted as working electrode and lithium disks acted as reference and counterelectrodes. The cells were allowed to relax during 12 h before recording the spectra. The measurements are performed for as-prepared sample and after reaction with lithium. The impedance spectra were recorded by perturbing the equilibrium potential by an AC voltage signal of 5 mV, which was applied from 100 kHz to 2 mHz.
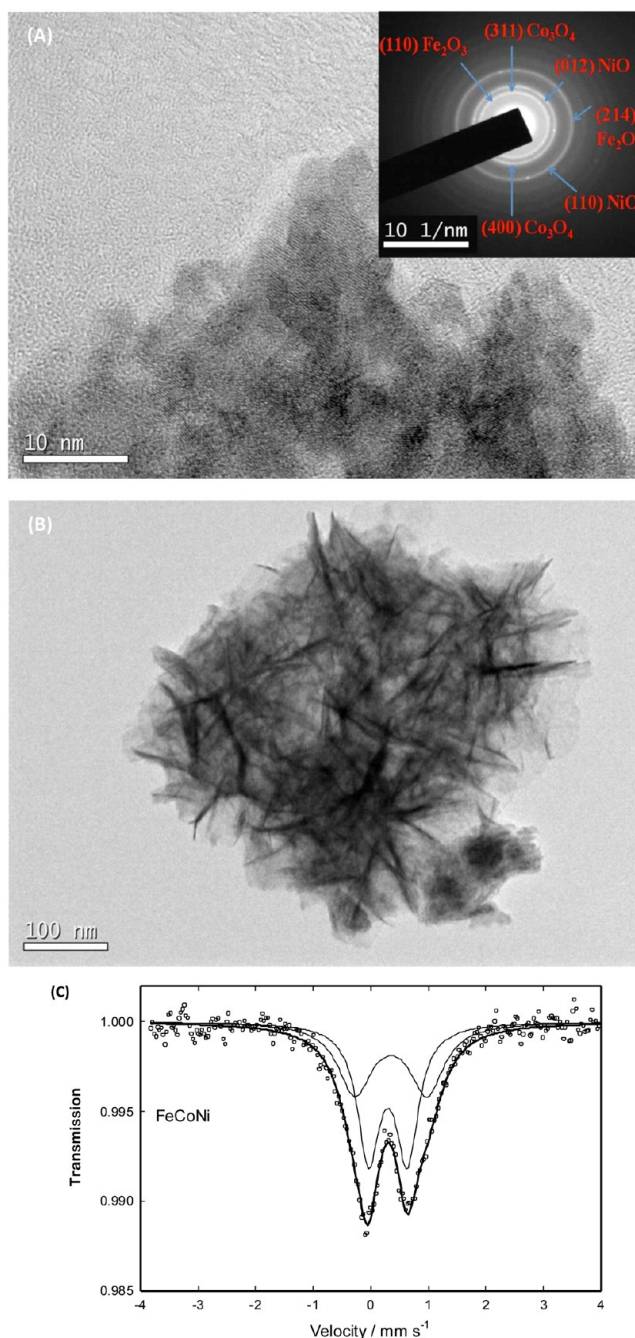
■ RESULTS AND DISCUSSION

Previously reported XRD patterns of oxidized FeCoNi-based films[15] evidenced an X-ray amorphous character because reflections of oxide nanoparticles are not observed, suggesting that they are most likely smaller than the X-ray coherence length. To confirm the X-ray amorphous nature of the films, GISAXRD was used in this study, which is particularly useful for thin-film materials. In addition, for the characterization of Fe-containing species and in order to avoid the high absorption and iron fluorescence with Cu Kα radiation (1.5456 Å), we have used Mo Kα radiation and the peaks of oxidized metal oxides were not observed (Figure 1). Even under these favorable conditions, solely reflections ascribable to Ti substrate (JPDS # 05-0682 with S.G.: P63/mmc) are observed and are marked in Figure 1. However, a distinctive color was indicative of deposits on the Ti foil.[15] According to our previous work, the energy-dispersive X-ray spectroscopy analysis revealed about 40 at. % Fe, 37 at. % Co, and 23 at. % Ni. Typical scanning electron microscopy (SEM) images of deposits fabricated for 240 s confirmed a film thickness of 1.5−1.6 μm (Figure 1B). It can be seen that FeCoNi-based film exhibits a rough texture and seems to be made up of several nanosheets that are interconnected and form a microporous structure. The high-resolution transmission electron microscopy (HRTEM) image in Figure 2A reveals that the structure of the material deposited and annealed at short time consists of very few nanocrystallites with grain size ranging between 5 and 10 nm. The
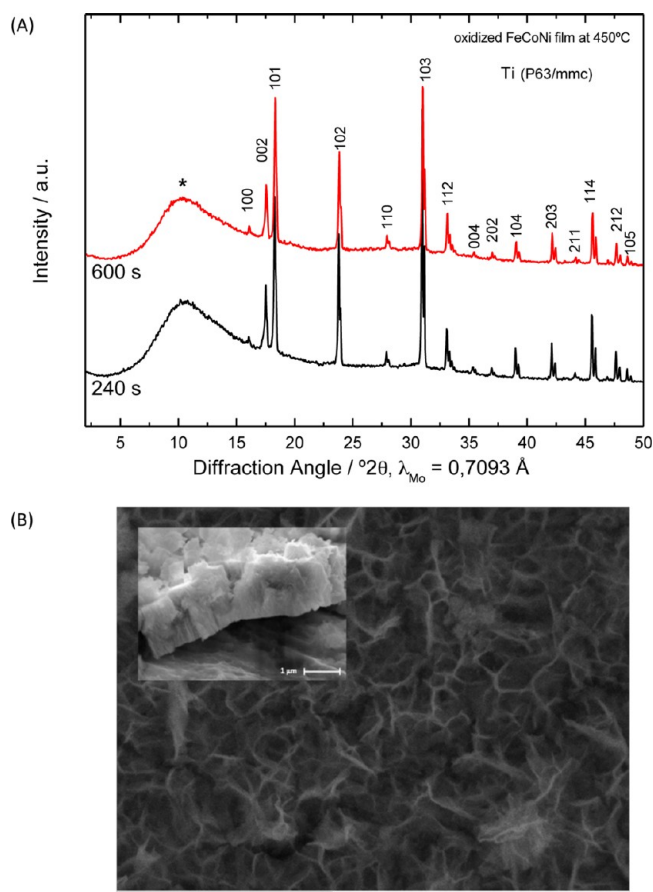
Figure 1. (A) X-ray diffraction patterns of oxidized FeCoNi-based materials fabricated at different deposition times (240 and 600 s) using Mo Kα radiation. Asterisk symbol represent the signal of the sample holder. (B) SEM image (for 240 s) of thin film from top view and cross section views.

Figure 2. (A) HRTEM image and (inset) the corresponding diffraction electron diagram of oxidized FeCoNi-based electrode (deposition time = 240 s followed by mild annealing for 2 h at 450 °C). (B) TEM image at low magnification. (C) ^{57}Fe Mössbauer spectrum of electrodeposited-oxidized FeCoNi-based material.

measurements along the sample confirmed that the lattice fringes are not so visible as opposed to crystalline powders; however, in some regions it was possible to observe clearer lattice fringes indicating that this material is not completely amorphous, but neither highly crystalline in nature. The corresponding electron diffraction pattern in the inset of Figure 2A reveals the Debye circles ascribable to (311) and (400) reflections of Co_3O_4, (012) and (110) reflections of NiO, and (110) and (214) reflections of Fe_2O_3 in good agreement with further characterizations as discussed next. TEM image at low magnification confirmed that samples are composed of desert rose-like microstructures of ca. 300 nm formed by submicrometer-sized plates of ca. 100 nm (Figure 2B).

The oxidation state and local environment of iron atoms were determined by ^{57}Fe Mössbauer spectroscopy (Figure 2C). The spectrum profile was deconvoluted in two doublets at 0.30(1) and 0.35(5) mm s^{-1}. These isomer shift values are ascribed to the presence of trivalent iron. The absence of sextets reveals the superparamagnetic character of the sample, which is closely related to the nanocrystalline character of this material. In turn, the occurrence of two doublets with a different quadrupole splitting, namely, 0.47(3) and 0.71(6) mm s^{-1}, respectively, involves the location of iron atoms in two different environments. Similar results have been reported in amorphous iron containing oxides electrochemically prepared by lithium-driven conversion reactions. In that case, the

assignment of the doublets to crystallographic positions was evidently discarded. In fact, both signals were respectively assigned to iron atoms located at the bulk and at the surface of the particles.[19] The relative contributions of these signals in the spectra of Figure 2C are 55.5 and 45.5% for bulk and surface iron, respectively. The amorphous character of the pristine thin film oxides is similar to that of other cycled conversion electrodes. It allows predicting that the large irreversibility observed in the first discharge of crystalline oxides should be minimized in these thin-film samples.
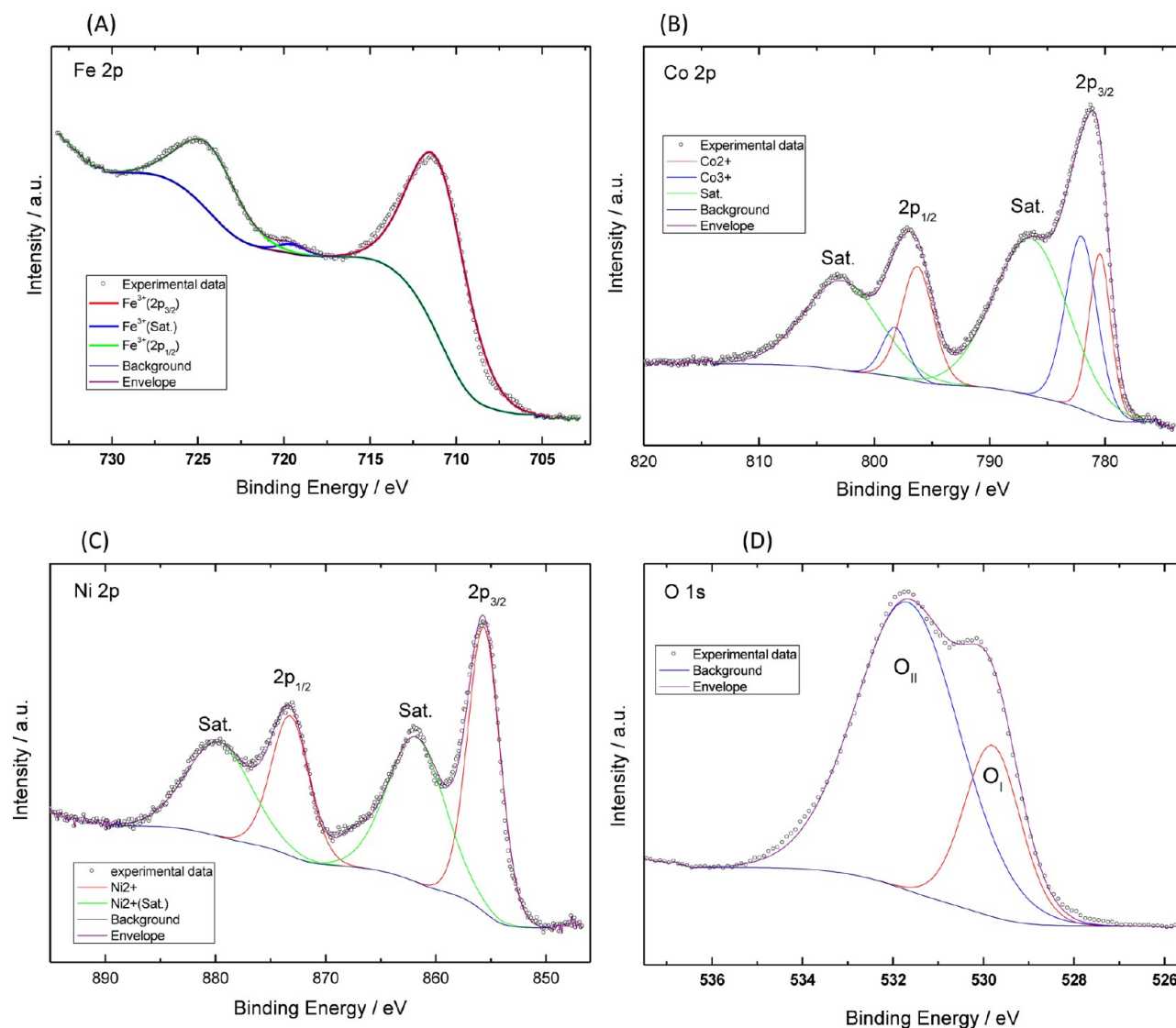
Figure 3. (A) Fe 2p XPS, (B) Co 2p XPS, (C) Ni 2p XPS, and (D) O 1s spectra for the electroplated FeCoNi film oxidized at 450 °C in air for 2 h.

Surface analysis of as-prepared oxidized FeCoNi porous film at 450 °C was checked by XPS (Figure 3A−D). The Fe 2p core levels are split into $2p_{1/2}$ and $2p_{3/2}$ components, due to the spin−orbit coupling. A peak is found at a binding energy of about 711.4 eV. This peak is due to the occurrence of iron(III) oxide (denoted as Fe^{3+}).[20,21] The energetic distance between orbitals accounted around 13.4 eV. As found in Fe_2O_3-containing materials,[22,23] the shakeup satellite line characteristic for the Fe^{3+} species is visible at 719 eV in Figure 3A. The emission lines of Co 2p show a complex profile containing spin−orbit-doublets and satellites for all oxidation states. For the sake of clarity, satellite bands were adjusted with one peak. Meanwhile, the signals of $2p_{3/2}$ and $2p_{1/2}$ were adjusted accordingly with the presence of Co^{2+} and Co^{3+} ions at binding energies of 780 and 782 eV, and 796 and 798 eV, respectively. Then, the Co 2p XPS region resembles that recorded from Co_3O_4.[24,25] XRD pattern (not shown) of electrodeposited-oxidized Co film at 450 °C was used as a blank, and as a result the presence of oxidized Co (denoted as Co^{2+} and Co^{3+}) was confirmed. The Ni 2p spectra in Figure 3C with the Ni $2p_{3/2}$ peak at 856 eV and Ni $2p_{1/2}$ peak at 873.4 eV entail the presence of Ni ions in the divalent state.[26,27] The O 1s

spectrum can be well deconvoluted into two components, O_I at 529.8 eV and O_{II} at 531.6 eV. The former is ascribable to oxygen located in metal oxides (e.g., Co_3O_4),[24] where we can assign the signal to the mixture of metal oxides in our film (Fe_2O_3, Co_3O_4, and NiO), whereas the latter is ascribed to nonstoichiometric surface oxygen.[24,28]

Galvanostatic discharge/charge and cyclic voltammetry (CV) techniques were used to determine the electrochemical properties of metal oxides (Figures 4 and 5). Galvanostatic tests shown in Figure 4A of electrodeposited-oxidized FeCoNi-based electrodes confirmed the good electrochemical performance in terms of first-cycle reversibility and minimal discharge polarization as earlier reported.[15] Control samples, based on binary alloys (electrodeposited and oxidized FeCo, CoNi, and FeNi-based films), have been prepared for comparative purposes, and the results of electrochemical tests are shown in Figure 4A,B. Oxidized FeCo-, FeNi-, and CoNi-based films showed a typical conversion reaction behavior of metal oxides. A high irreversibility from first to second cycles of about 27 and 34% is observed for FeCo and CoNi, respectively. FeNi-based films presented a better electrochemical behavior in terms of minimal discharge polarization (placed in first and successive
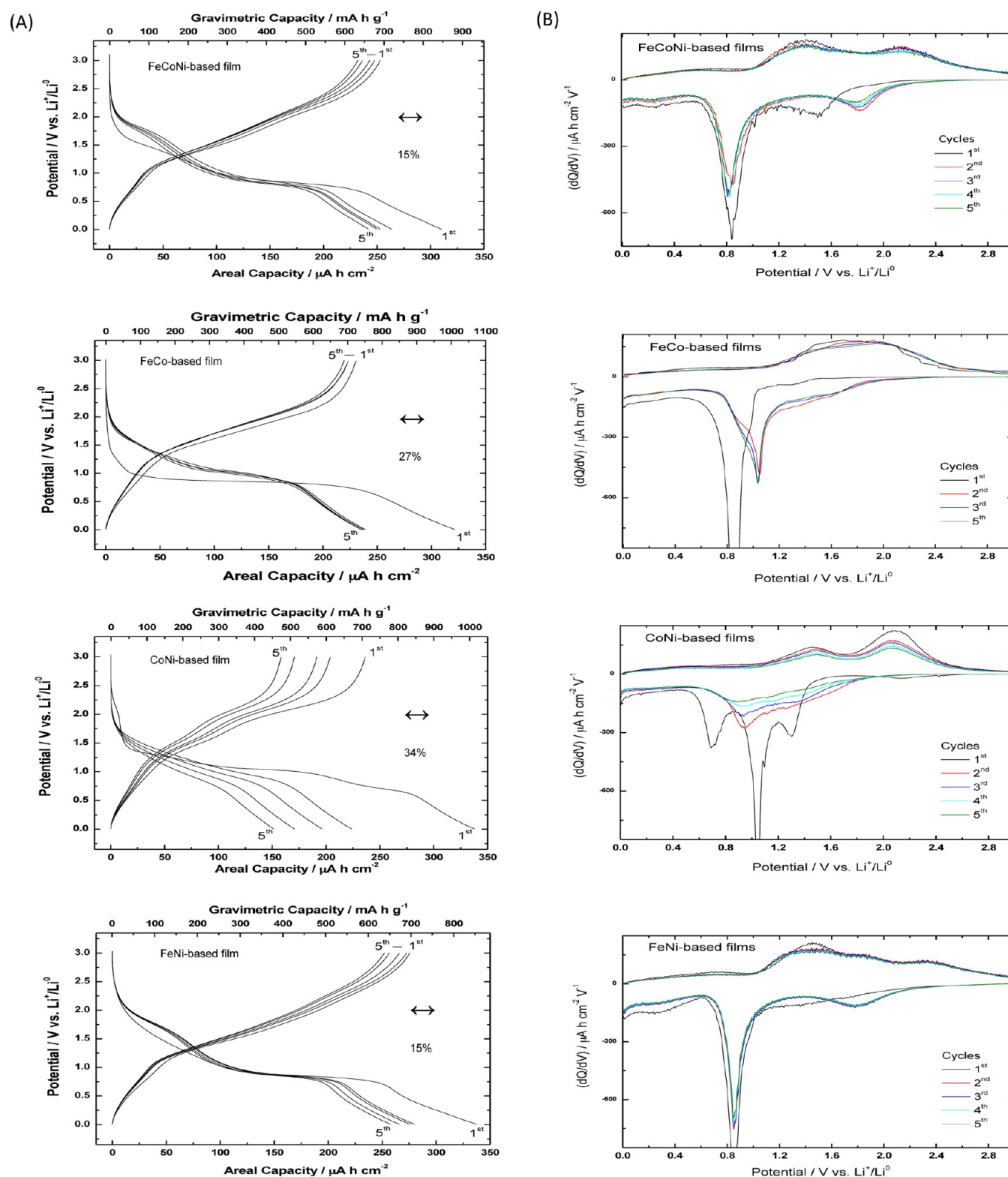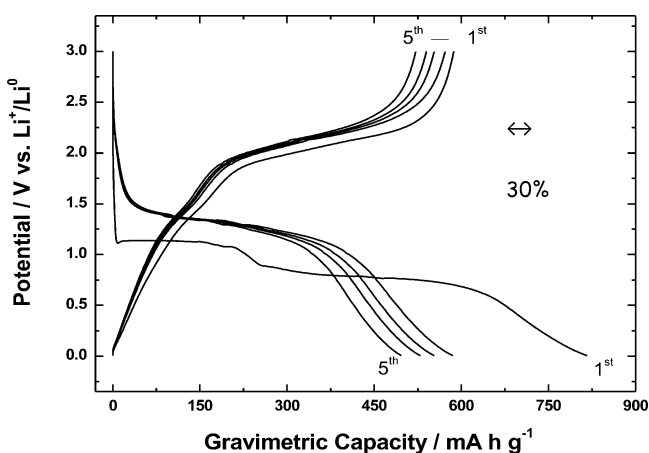
Figure 4. (A) Typical galvanostatic discharge/charge curves of the first five cycles of an oxidized FeCoNi-based films, oxidized FeCo-based film, oxidized CoNi-based film, and oxidized FeNi-based films deposited on Ti foils. (B) Derivative curve of previous figures.

discharges at about 0.75−0.85 V) and low irreversible capacity of about 15% from first to second cycle. The derivative curves revealed the occurrence of different reactions on discharge as will be discussed below (Figure 4B). Thus, for binary films there is a shift in the potential of the reaction from first to second discharge that varied from almost 0 up to 0.4 V, with

the lowest value being found for FeNi-based films. For FeCoNi-based films, the voltage shift is almost negligible, irrespective of the presence of cobalt in the composition.

In addition, a galvanostatic profile of a mixture of commercial oxide products during the first 5 cycles (referred as a mixture of Fe^{3+}, Ni^{2+}, Co^{2+}, and Co^{3+} ions) is shown in Figure 5. The
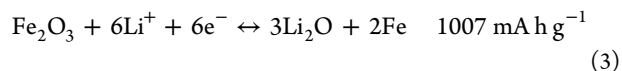
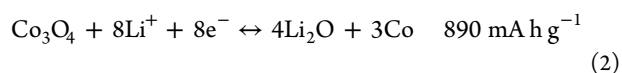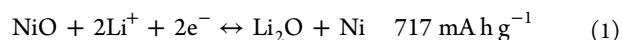**Figure 5.** (A) Galvanostatic discharge of a mixture of crystalline Fe, Co, and Ni oxides from commercial products.

$$NiO + 2Li^+ + 2e^- \leftrightarrow Li_2O + Ni \quad 717\ mA\ h\ g^{-1} \quad (1)$$

$$Co_3O_4 + 8Li^+ + 8e^- \leftrightarrow 4Li_2O + 3Co \quad 890\ mA\ h\ g^{-1} \quad (2)$$

$$Fe_2O_3 + 6Li^+ + 6e^- \leftrightarrow 3Li_2O + 2Fe \quad 1007\ mA\ h\ g^{-1} \quad (3)$$

For the FeCoNi-based film electrodes with the atomic ratio discussed above, it can be assumed that the lithium reaction proceeds as a combination of the above reactions, as follows:

$$0.23NiO + 0.12Co_3O_4 + 0.2Fe_2O_3 + 2.62Li^+ + 2.62e^-$$
$$\rightarrow 1.31Li_2O + 0.23Ni + 0.36Co + 0.4Fe \quad (4)$$

The theoretical capacity of our tested hybrid oxide material is 900 mA h g^{-1}. Comparable values of capacity in the first discharge of about 845 mA h g^{-1} (~200 μA h cm^{-2} μm^{-1}, Figure 4A) for FeCoNi-based film and 830 mA h g^{-1} (Figure 5) for a mixture of commercial oxides were obtained. However, these values after the second cycle differed. For the former, the first reversible capacity was 720 mA h g^{-1} (~170 μA h cm^{-2} μm^{-1}) and efficiency in the first cycle achieved 85%, whereas the latter solely retained 70%. These values may be indicative of the presence of an extra process taking place, as discussed below.

There are three components that can contribute to the total charge stored in a cell: (i) the faradic part from the lithium conversion process, (ii) the faradic part from the charge-transfer process with surface atoms, referred to as pseudocapacitance,[18] and (iii) the nonfaradic part from the double-layer effect. The capacitive effects in our system can be characterized by analyzing the cyclic voltammetry data shown in Figure 5. Considering the following equation,

$$i = a\nu^b \quad (5)$$

where ν represents the scan rate and a and b are adjustable parameters,[29] a parameter b is directly determined from the slope of the plot of log i versus log ν (see Figure 6). Generally, if the slope b equals 1, a surface redox reaction involving nondiffusion-controlled processes ($i = a\nu$) is expected; meanwhile for the ideal diffusion-controlled faradaic process, the slope b equals 1/2 and satisfies Cottrell's equation ($i = a\nu^{1/2}$).[16] The data of the oxidized FeCoNi-based films of the b-values are shown in Figure 7. Thus, in this way we analyzed the kind of stored charge along the voltage windows 2.0–0.05 V for the first, second, fifth, and tenth cycles simply by analyzing the b-value at each potential (herein was calculated for each 0.05 V). So, the so-called "conversion reaction" at about 0.85–0.75 V is mostly a faradic process (with $b = 0.5$) for first and successive discharges. At 1.5 V is also visible a faradic process taking place in the first discharge, most probably associated to the electrolyte decomposition and formation of the SEI passivation layer. The latter is known to provide irreversible capacity to the cell. At lower voltage (<0.55 V) appears a predominant capacitive-like storage behavior with b ranging between 0.75 and 1.0. On second and successive discharges, the b-value profile differs in the 1.2–1.75 V regions for which the kind of stored charge is predominantly from a capacitive origin. Attending to the high reversibility observed from first to second discharge (~85%), we are able to deduce that there is a new sort of reaction capable of reversible storage capacity that begins exclusively in the second discharge. Moreover, it can be
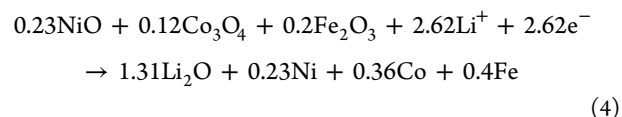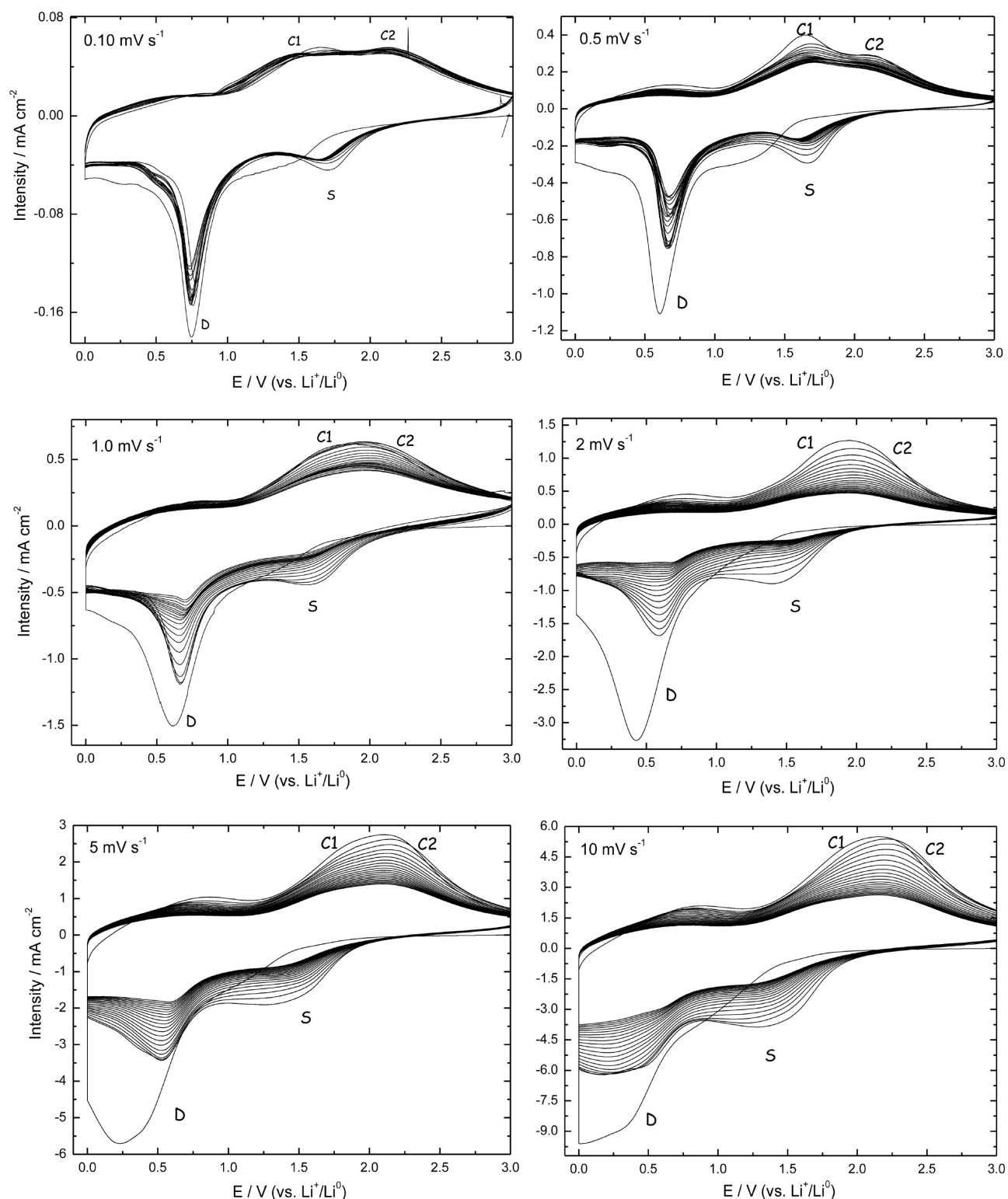
differences between their electrochemical behaviors reside in the following aspects: (i) In the former no changes are observed in the position of voltage plateau taking place at 0.85–0.75 V for first and successive discharges. Meanwhile, in commercial products (mixture of metal oxides with high particle size) a difference of about 0.4 V is observed between first and second reduction, a common characteristic occurring for materials with a high crystalline character indicative of a drastic change in particles size.[5,13] (ii) The occurrence of a new broad band at around 1.75–1.5 V in second and successive discharges is observed in our electrodeposited FeCoNi-based film. This fact was not observed in crystalline powders[5,13] and seems to be responsible for providing an additional capacity to the cell, thus enhancing a Coulombic reversibility in the first cycle (~85–87%),[15] whereas for crystalline metal oxide compounds the inefficiency is as high as 30% (Figure 5).[13] The reasons why the oxidized FeCoNi-based material, which is deposited during a short time (240 s) and current density of −2.5 mA cm^{-2}, has better capacity retention in Li test cell are (i) low activation energy required to form the M–Li$_2$O aggregates and (ii) better accessibility of Li$^+$ ions to the complete mass of active material. Both properties are enhanced by the nanocrystalline thin-film character of the starting material. The effects and origin of such behavior will be discussed next.

A set of cyclic voltammograms were performed for a FeCoNi-based porous film at various sweep rates from 0.1 to 10 mV s^{-1} during the first 20 cycles (Figure 6). Typically, the area under the curves represents the total stored charge that arises from both faradic and nonfaradic processes. The cathodic/anodic peaks represent the lithium conversion/deconversion behavior in the metal oxides that occurs at voltages similar to those shown in Figure 4A,B. It should be noted that the total stored charge in the mixture of oxide film is strongly dependent on the sweep rate as well as the shifting of the main peaks during reduction (denoted as "D and S-peaks" in Figure 6). As the sweep rate decreases, the total amount of stored charge increases. This indicates that full storage capacity has not been reached at the given sweep rates because of kinetic limitations associated with the diffusion of Li$^+$ through the oxidized FeCoNi-based films.

Plausible electrochemical conversion reactions of Li with each individual metal oxide and their theoretical capacity are

51

dx.doi.org/10.1021/sc300096s | ACS Sustainable Chem. Eng. 2013, 1, 46−56

Figure 6. Cyclic voltammograms during the first 20 cycles of oxidized FeCoNi-based porous film electrodes at sweep rates of 0.1, 0.5, 1, 2, 5, and 10 mV s^{-1}.

said that the loss of capacity given by the irreversible consumption of lithium for the electrolyte decomposition minimized a new capacitive process located between ca. 1.75–1.5 V distinguishable by a new broad peak (Figures 4 and 5).

To further understand the origin of the charge-storage behavior and first-cycle reversibility of the FeCoNi-based electrodes, the separation of possible capacitive and faradic contributions to the total stored charge is carried out. From cyclic voltammograms recorded at different scan rates (Figure 6), the analysis of these results allows for discerning the faradic contribution due to diffusion-controlled reactions such as the conversion reaction, from the possible pseudocapacitive and double-layer contributions, that cannot be separated, according to Brezesinski et al.[17,30] To corroborate these results, we have
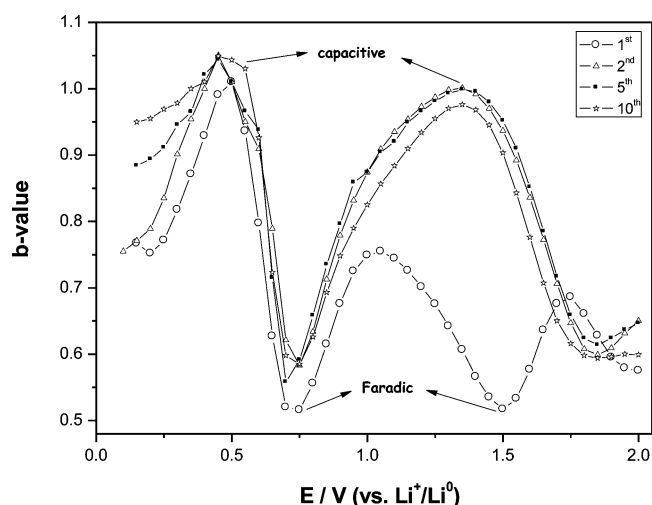
Figure 7. *b*-Values for the electrodeposited-oxidized FeCoNi film plotted as a function of potential for reduction sweeps (Li$^+$ insertion) for the first, second, fifth, and tenth cycles.

based our theoretical calculations considering that at a fixed potential the current response is equal to the diffusion–controlled conversion process plus surface capacitive effects. Thus, by determining parameters such as y_1 and y_2, we are able to quantify, at specific potentials, the fraction of the current due

to each of these contributions, as expressed by the following equations:[30]

$$i(V) = y_1\nu + y_2\nu^{1/2} \tag{6}$$

or

$$\frac{i(V)}{\nu^{1/2}} = y_1\nu^{1/2} + y_2 \tag{7}$$

In Figure 8D we plotted the sweep-rate dependence of the current according to eq 7 for selected potentials of 1.6, 1.15, and 0.8 V.[31] The observed linear behavior enables us to determine y_1 and y_2 parameters from the slope and the *y*-axis intercept point of a straight line, respectively. From this procedure, we are able to distinguish quantitatively between the currents arising from lithium-ion conversion reaction and those occurring from capacitive processes. Figure 8A–C depicts the current contribution of different cycles at different scan rates expressing the total stored charge divided as conversion reaction and capacitance. A high faradic contribution (80–85%) is found specially when using slow sweep rates (e.g., 0.5 mV s^{-1}). The discrepancy in charge storage for the two different mechanisms becomes more obvious at higher sweep rates (2–10 mV s^{-1}) because of the rapid charge/discharge characteristics related with capacitive processes. From the current distribution at different discharges, it is possible to
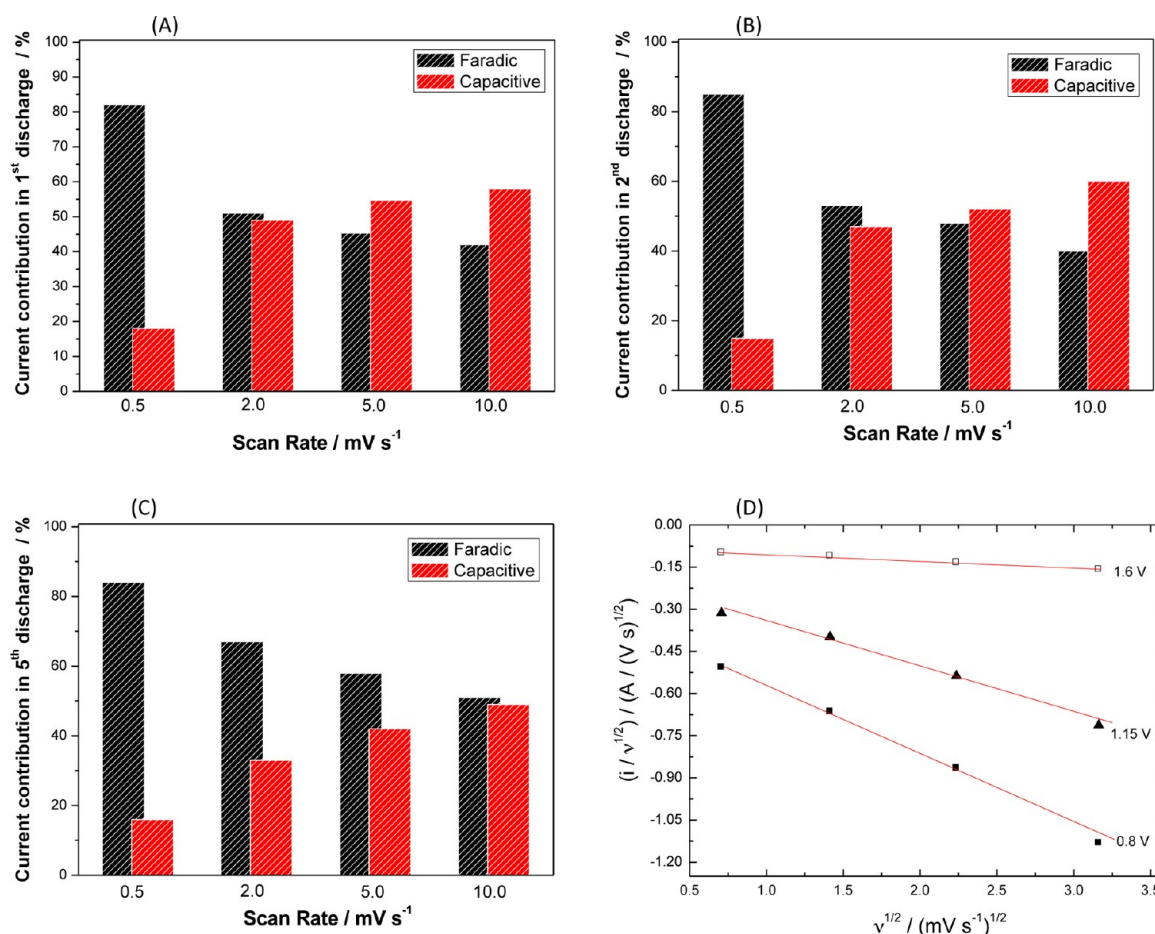

Figure 8. (A–C) Comparison of charge storage for electrodeposited-oxidized FeCoNi film as a function of the sweep rate. The total charge is separated into lithium-reduction reaction (denoted as conversion reaction) and capacitive contributions. (D) Some details of the fitting from eq 4 served to analyze the cathodic voltammetric sweep data for the electrodeposited FeCoNi-based film at 1.6, 1.15, and 0.8 V during the first discharge.

observe the latter behavior, obtaining for instance a capacitive contribution closer to 50% at 10 mV s^{-1} in the second cycle.

The Brunauer−Emmett−Teller (BET) surface area of the electroplated and oxidized FeCoNi-based electrode reached 68 m^2 g^{-1}. Nitrogen adsorption isotherm (Figure 9) reveals a type
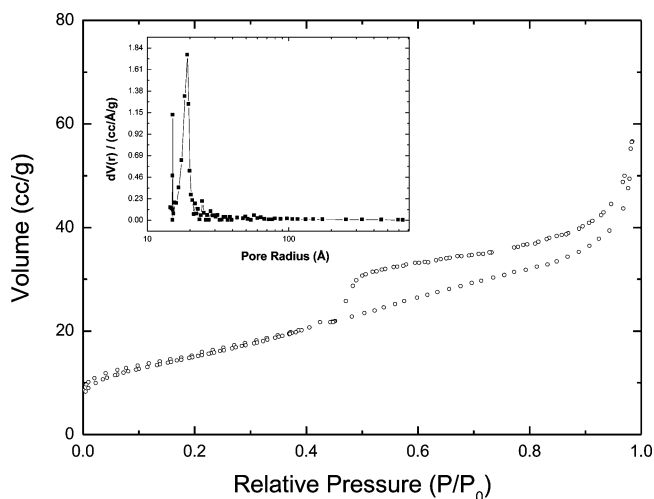

Figure 9. Nitrogen adsorption−desorption isotherms of the electro-deposited oxidized FeCoNi-based films and pore-size distribution curve obtained from the desorption data (inset).

IIb shape (IUPAC classification). The average pore size and pore volume obtained from Barrett−Joyner−Halenda (BJH) method are 19.3 Å and Vp = 0.09 cc/g, respectively. This isotherm can be related to a limited microporosity. Herein, to characterize the electrochemical capacitive properties of FeCoNi-based electrode, cyclic voltammograms (CV) were carried out in 1.5 M KOH aqueous solution. Figure 10A shows the curves of the 450 °C FeCoNi-based nanosheets at different scan rates. The boxlike shape of these curves indicates nearly ideally capacitive behaviors for the sweeps rates from 1 to 50 mV s^{-1}. This confirms the good high-rate capability of the FeCoNi-based films. Figure 10B represents the specific capacitance as a function of the cycle number at different sweep rate. At slow rates it exhibits high specific capacitance of about 600−500 during the first 100 cycles for 1 mV s^{-1}, which is a good value comparable to cobalt oxides or nickel oxides in previous reports.[3,32] The long-term stability of oxidized FeCoNi-based electrodes has been examined by potentiody-namic charge−discharge cycling up to 1800 cycles using a variable sweep rate (Figure 10B). It is apparent that specific capacitance values changed on increasing the rate. The capacity decreased constantly until 230 F g^{-1} for 2 mV s^{-1} after 400 cycles, 105 F g^{-1} for 5 mV s^{-1} (600 cycles), 60 F g^{-1} for 10 mV s^{-1} (800 cycles), 35 F g^{-1} for 20 mV s^{-1} (1000 cycles), and 20 F g^{-1} for 50 mV s^{-1} (1200 cycles); and increased up to 350 F g^{-1} for 2 mV s^{-1} after 1800 cycles, respectively. A full recovery of capacity was achieved when restoring the initial 2 mV s^{-1} sweep rate from 50 mV s^{-1}.

Figure 11 shows the impedance spectra (Nyquist plots) recorded for an as-prepared three-electrode lithium test cell and during the discharge of the same cell to 0.005 V. Table 1 schematizes the equivalent circuit for each fitting and gives the resistance values. The spectrum of the unused film electrode reveals a semicircle and a straight line with ca. 45° slope. These features are respectively ascribed to a charge-transfer
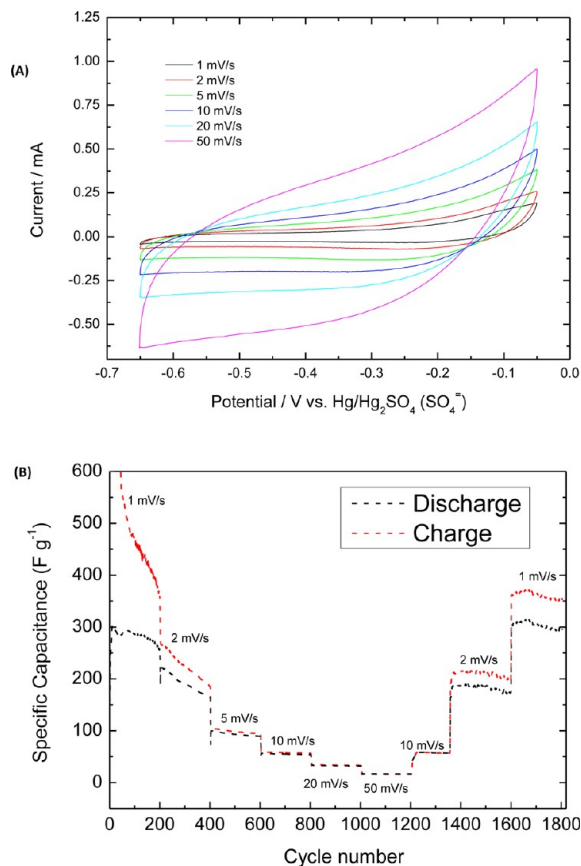
Figure 10. (A) CV curves and (B) specific capacitance as a function of cycle number of FeCoNi-based electrodes oxidized at 450 °C at different scan rates (1−50 mV s^{-1}) using 1.5 M of KOH as the electrolyte.
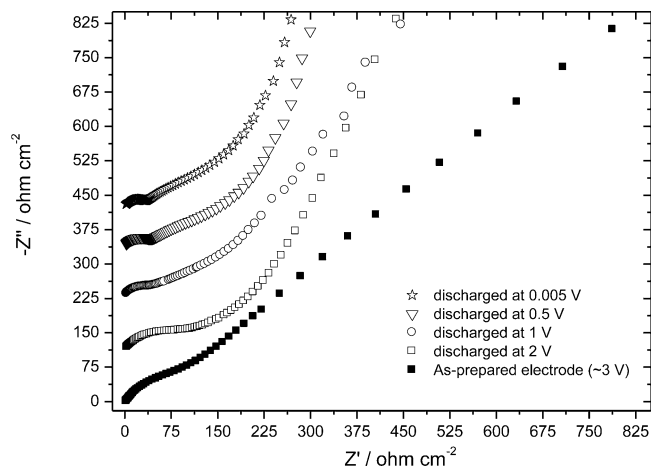
Figure 11. Nyquist plots of oxidized FeCoNi-based electrodes measured at open circuit potential (Randless-like behavior) and in the discharged state (3−0.005 V).

phenomenon at the electrode interphase and lithium-diffusion processes inside the electrode particles. This behavior is known as Randless-like behavior, and when this phenomenon takes place,[33] whatever the charge−discharge mechanism of the electrode material, it can be reversibly charged or discharged in homogeneous phases. The conductivity of the unused oxidized FeCoNi-based electrode can be calculated from the charge-transfer resistance value. A value of 1.4×10^{-6} S cm^{-1} is

Table 1. Fitted Parameters for the Electrochemical Impedance Spectra of As-Prepared FeCoNi-Based Electrodes and after Discharge of the Same Cell until 0.005 V[a]

potential (V)	3	2	1	0.5	0.005
equivalent circuit	$[R_E(R_{CT}Q)W]$	$[R_E(R_{CT}Q)W]$	$[R_E(R_{SF}Q_1)(R_{CT}Q_2)W]$	$[R_E(R_{SF}Q_1)(R_{CT}Q_2)W]$	$[R_E(R_{SF}Q_1)(R_{CT}Q_2)W]$
resistance (ohm cm^{-2})	$R_{CT} = 190$	$R_{CT} = 144$	$R_{CT} = 70$	$R_{CT} = 64$	$R_{CT} = 66$

[a]Note: "R_E, R_{CT}, and R_{SF}" represent the resistance values for the electrolyte, charge transfer, and lithium migration through inorganic surface film. "Q" denotes a constant phase element, which represents a circuit parameter with behavior between pure capacitor and resistance. "W" denotes a Warburg-type element.

obtained, which is higher than that reported for single crystals of stoichoimetric NiO [$<10^{-13}$ S cm^{-1}][34] or α-Fe$_2$O$_3$ [$<10^{-13}$ S cm^{-1}].[35] However, it is still lower than that of NiO with high density of Ni^{2+} vacancies (1.8×10^{-5} S cm^{-1}).[36] On discharging, a new semicircle appears at high frequencies, being related to the occurrence of a passivation film. Otherwise, the second semicircle at low frequencies remains ascribable to the charge-transfer reaction at the interface. During the discharge, the charge-transfer resistance decreases from 190 to 66 ohm cm^{-2}, as expected from the reduction of the active electrode material to the transition metals (Table 1).

The good performance of FeCoNi-based nanosheets may be attributed to the following:

(1) Formation of a network structure from an interconnection between the nanosheets. The porous structure and the large open space between them can provide sites for the adsorption of ions and also help the fast intercalation and deintercalation of active species. Moreover, the baggy porous texture and huge space among individual nanosheets can facilitate the penetration of electrolytes into the inner part and reduce the ionic diffusion path.

(2) Good electric contact between the active material and Ti substrate. Generally, it can provide intimate electric contact, which not only is favorable for electrons to transport between active material and current collector but also guarantees them to participate as much as possible in reactions.

(3) Enhancement of the electric conductivity by the presence of Ni as verified in previous studies where for instance the addition of Ni in spinel-type cobalt oxides increased the conductivity almost 5 times.[37]

Generally speaking, the electronic conductivity, morphology, the exposed surface area, crystal structure, and defect chemistry (e.g., cation distribution and oxidation states) of the metal oxides used here considerably influence the performance of pseudocapacitor and anode of the battery (capacitance and charge/discharge rate). All these features may be modified by varying the deposition parameters and/or heat treatment. So, the results presented here proved to be very successful for improving performances and open novel concepts in materials research. Indeed, electropolymerization of copolymer electrolyte into titania nanotubes supported on Ti substrates is a subject of study for high-performance 3D microbatteries fabricated with electrochemical procedures.[38]

CONCLUSIONS

Electrodeposition followed by mild annealing of a mixture of Fe, Co, and Ni leads to the formation of 1.5−1.6 μm film forming a network microstructure with interconnected nanosheets. The chemical characterization confirmed that ectrodeposited FeCoNi-based electrode has an X-ray amorphous character. The ^{57}Fe Mössbauer and XPS surface analysis established the presence of Fe^{3+}, Ni^{2+}, Co^{3+}, and Co^{2+} ions.

HRTEM confirmed the nanocrystalline character of a mixture of oxides. Galvanostatic cycling behavior in Li cells manifested important differences as compared to crystalline samples in terms of first-cycle reversibility and minimal discharge polarization. A reversible capacity of 720 mA h g^{-1} ($\sim$170 μA h cm^{-2} μm^{-1}) is reported for a material free of additives (binders and carbon black), which is higher than those of pure graphite (372 mA h g^{-1}), making this material very attractive for future battery designs. The reversible capacity accounted from first to second cycle is around 85% versus 70% for crystalline electrodes. The reasons why our nanocrystalline material has better capacity retention are the low activation energy required to form the M−Li$_2$O aggregates and the better accessibility of Li$^+$ ions to the complete mass of active material. It is demonstrated that faradic reactions occur at 0.8 V. Moreover, part of the increased reversibility from first to second cycle resides in the occurrence of a new process starting in the second discharge, which has a pseudocapacitive behavior. Given a surface area of 68 m^2 g^{-1} and small particle size, this origin is reasonable and discards a double-layer effects. Aside from typical faradic reaction at 0.8 V, we have proven that capacitive energy storage can occur not only in organic but also in aqueous solution with capacitive values of about 600 F g^{-1} for 1 mV s^{-1}.

AUTHOR INFORMATION

Corresponding Author
*E-mail: q72maorg@uco.es. Tel.: +34 957 21 86 37. Fax: +34 957 21 86 21.

Notes
The authors declare no competing financial interest.

REFERENCES

(1) Zheng, M.; Cao, J.; Liao, S.; Liu., J.; Chen, H.; Zhao, Y.; Dai, W.; Ji, G.; Tao, J. Preparation of mesoporous Co$_3$O$_4$ nanoparticles via solid−liquid route and effects of calcination temperature and textural parameters on their electrochemical capacitive behaviors. *J. Phys. Chem. C* **2009**, *113*, 3887−3894.

(2) Xu, C. H.; Sun, J.; Gao, L. Controllable synthesis of triangle taper-like cobalt hydroxide and cobalt oxide. *CrystEngComm.* **2011**, *13*, 1586−1590.

(3) Pang, H.; Lu, Q. Y.; Zhang, Y. Z.; Li, Y. C.; Gao, F. Selective synthesis of nickel oxide nanowires and length effect on their electrochemical properties. *Nanoscale* **2010**, *2*, 920−922.

55

dx.doi.org/10.1021/sc300096s | *ACS Sustainable Chem. Eng.* 2013, 1, 46−56

(4) Zhu, T.; Chen, J. S.; Lou, X. W. Shape-controlled synthesis of porous Co_3O_4 nanostructures for application in supercapacitors. *J. Mater. Chem.* **2010**, *20*, 7015−7020.

(5) Poizot, P.; Laruelle, S.; Grugeon, S.; Dupont, L.; Tarascon, J. M. Nano-sized transition-metaloxides as negative-electrode materials for lithium-ion batteries. *Nature* **2000**, *407*, 496−499.

(6) Balaya, P.; Bhattacharyya, A. J.; Jamnik, J.; Zhukovskii, Y. F.; Kotomin, E. A.; Maier, J. Nano-ionics in the context of lithium batteries. *J. Power Sources* **2006**, *159*, 171−178.

(7) Grugeon, S.; Laruelle, S.; Dupont, L.; Tarascon, J. M. An update on the reactivity of nanoparticles Co-based compounds towards Li. *Solid State Sci.* **2003**, *5*, 895−904.

(8) Jamnik, J.; Maier, J. Nanocrystallinity effects in lithium battery materials—Aspects of nano-ionics. Part IV. *Phys. Chem. Chem. Phys.* **2003**, *5*, 5215−5220.

(9) Zhukovskii, Y. F.; Balaya, P.; Kotomin, E. A.; Maier, J. Evidence for interfacial-storage anomaly in nanocomposites for lithium batteries from first-principles simulations. *Phys. Rev. Lett.* **2006**, *96*, 058302.

(10) Miller, J. R.; Simon, P. Materials science—Electrochemical capacitors for energy management. *Science* **2008**, *1*, 651−652.

(11) Yuan, D.; Zhou, T. X.; Zhou, S. L.; Mo, S. S.; Xia, N. N. Nitrogen-enriched carbon nanowires from the direct carbonization of polyaniline nanowires and its electrochemical properties. *Electrochem. Commun.* **2011**, *13*, 242−246.

(12) Zhao, X.; Sánchez, B. M.; Dobson, P. J.; Grant, P. S. The role of nanomaterials in redox-based supercapacitors for next generation energy storage devices. *Nanoscale* **2011**, *3*, 839−855.

(13) Lavela, P.; Tirado, J. L. $CoFe_2O_4$ and $NiFe_2O_4$ synthesized by sol−gel procedures for their use as anode materials for Li ion batteries. *J. Power Sources* **2007**, *172*, 379−387.

(14) Ortiz, G. F.; Hanzu, I.; Lavela, P.; Knauth, P.; Tirado, J. L.; Djenizian, T. Nanoarchitectured TiO_2/SnO: A future negative electrode for high power density Li-ion microbatteries? *Chem. Mater.* **2010**, *22*, 1926−1932.

(15) Ortiz, G. F.; Tirado, J. L. Oxidized FeCoNi alloys as novel anode in Li-ion batteries. *Electrochem. Commun.* **2011**, *13*, 1427−1430.

(16) Wang, J.; Polleux, J.; Lim, J.; Dunn, B. Pseudocapacitive contributions to electrochemical energy storage in TiO_2 (anatase) nanoparticles. *J. Phys. Chem. C* **2007**, *111*, 14925−14931.

(17) Brezesinski, T.; Wang, J.; Polleux, J.; Dunn, B.; Tolbert, S. H. Templated nanocrystal-based porous TiO_2 films for next-generation electrochemical capacitors. *J. Am. Chem. Soc.* **2009**, *131*, 1802−1809.

(18) Conway, B. E.; Birss, V.; Wojtowicz, J. The role and utilization of pseudocapacitance for energy storage by supercapacitors. *J. Power Sources* **1997**, *66*, 1−14.

(19) Alcántara, R.; Jaraba, M.; Lavela, P.; Tirado, J. L.; Jumas, J. C.; Olivier-Fourcade, J. Changes in oxidation state and magnetic order of iron atoms during the electrochemical reaction of lithium with $NiFe_2O_4$. *Electrochem. Commun.* **2003**, *5*, 16−21.

(20) McIntyre, N. S.; Zetaruk, D. G. X-ray photoelectron spectroscopic studies of iron oxides. *Anal. Chem.* **1977**, *49*, 1521−1529.

(21) Brundle, C. R.; Chang, T. J.; Wandelt, K. Core and valence level photoemission studies of iron-oxide surfaces and oxidation of iron. *Surf. Sci.* **1977**, *68*, 459−468.

(22) Weiss, W.; Ranke, W. Surface chemistry and catalysis on well-defined epitaxial iron-oxide layers. *Prog. Surf. Sci.* **2002**, *70*, 1−151.

(23) Fitzgerald, A. G.; Muir, G. Structural and compositional studies of sputtered nickel ferrite films. *Surf. Interface Anal.* **1986**, *8*, 247−251.

(24) Brundle, C. R.; Chuang, T. J.; Rice, D. W. X-ray photoemission study of interaction of oxygen and air with clean cobalt surfaces. *Surf. Sci.* **1976**, *60*, 286−300.

(25) Raquet, B.; Mamy, R.; Ousset, J. C.; Nègre, N.; Goiran, M.; Guerret-Piécourt, C. Preparation and magnetic properties of the CoO/Co bilayer. *J. Magn. Magn. Mater.* **1998**, *184*, 41−48.

(26) Schreifels, J. A.; Maybury, P. C.; Swartz, W. E. X-ray photoelectron-spectroscopy of nickel boride catalysts—Correlation of surface-states with reaction-products in the hydrogenation of acrylonitrile. *J. Catal.* **1980**, *65*, 195−206.

(27) Roginskaya, Y. E.; Morozova, O.; Lubnin, E.; Ulitina, Y. Y.; Lopukhova, G.; Trasatti, S. Characterization of bulk and surface composition of $Co_xNi_{1−x}O_y$ mixed oxides for electrocatalysis. *Langmuir* **1997**, *13*, 4621−4627.

(28) Kim, J. G.; Pugmire, D.; Battaglia, D.; Langell, M. Analysis of the $NiCo_2O_4$ spinel surface with Auger and X-ray photoelectron spectroscopy. *Appl. Surf. Sci.* **2000**, *165*, 70−84.

(29) Lindstrom, H.; Sodergren, S.; Solbrand, A.; Rensmo, H.; Hjelm, J.; Hagfeldt, A.; Lindquist, S. E. Li^+ ion insertion in TiO_2 (anatase). 2. Voltammetry on nanoporous films. *J. Phys. Chem. B* **1997**, *101*, 7717−7722.

(30) Aragón, M. J.; León, B.; Serrano, T.; Pérez-Vicente, C.; Tirado, J. L. Synergistic effects of transition metal substitution in conversion electrodes for lithium-ion batteries. *J. Mater. Chem.* **2011**, *21*, 10102−10107.

(31) Liu, T. C.; Pell, W. G.; Conway, B. E.; Roberson, S. L. Behavior of molybdenum nitrides as materials for electrochemical capacitors—Comparison with ruthenium oxide. *J. Electrochem. Soc.* **1998**, *145*, 1882.

(32) Cao, L.; Lu, M.; Li, H. L. Preparation of mesoporous nanocrystalline Co_3O_4 and its applicability of porosity to the formation of electrochemical capacitance. *J. Electrochem. Soc.* **2005**, *152*, A871−A875.

(33) Macdonald, J. R., Ed. *Impedance Spectroscopy, Emphasizing Solid Materials and Systems*; Wiley-Interscience: New York, 1987.

(34) Morin, F. J. Electrical properties of NiO. *Phys. Rev. B* **1954**, *93*, 1199−1204.

(35) Morin, F. J. Electrical properties of α-Fe_2O_3. *Phys. Rev. B* **1954**, *93*, 1195−1199.

(36) Biju, V.; Abdul Khadar, M. DC conductivity of consolidated nanoparticles of NiO. *Mater. Res. Bull.* **2001**, *36*, 21−33.

(37) Windisch, C. F.; Exarhos, G. J.; Ferris, K. F.; Engelhard, M. H.; Stewart, D. C. Infrared transparent spinel films with p-type conductivity. *Thin Solid Films* **2001**, *398*, 45−52.

(38) Amponsah, N. K.; Dumur, F.; Knauth, P.; Pecquenard, B.; Djenizian, T. Electropolymerization of copolymer electrolyte into titania nanotube electrodes for high-performance 3D microbatteries. *Electrochem. Commun.* **2011**, *13*, 894−897.